Computing Discrete Minimal Surfaces and Their Conjugates

Ulrich Pinkall and Konrad Polthier

CONTENTS

We present a new algorithm to compute stable discrete minimal surfaces bounded by a number of fixed or free boundary curves in $\mathbf{R}^3$, $\mathbf{S}^3$ and $\mathbf{H}^3$. The algorithm makes no restriction on the genus and can handle singular triangulations.

Additionally, we present an algorithm that, starting from a discrete harmonic map, gives a conjugate harmonic map. This can be applied to the identity map on a minimal surface to produce its conjugate minimal surface, a procedure that often yields unstable solutions to a free boundary value problem for minimal surfaces. Symmetry properties of boundary curves are respected during conjugation.

1. INTRODUCTION

Plateau's Problem was long an open problem of minimal surface theory. It asks for the existence of a disk-type minimal surface spanning a given closed boundary curve Γ in $\mathbf{R}^n$. The name honors the Belgian physicist J. A. Plateau, who did extensive experimental studies in the nineteenth century [Plateau 1873], convincing mathematicians of an affirmative solution to the question. But it was not until 1930 that a theoretical proof was found; earlier approaches had failed, including the use of the Weierstraß representation formulas and attempts to minimize the area functional

$$A(f) = \int_{\Omega} \text{Jacobian}(f)$$

in the class of parametric maps $f : \Omega \to \mathbf{R}^n$ with $f(\partial\Omega) = \Gamma$, where $\Omega \subset \mathbf{R}^2$ is a fixed disk-type domain.

Douglas [1931] and Radó [1930] at the same time had the ingenious idea to minimize not the area

1058-6458/93 $0.50 per page

functional directly but rather, in the later reformulation by Courant [1950], the Dirichlet integral

$$E_D(f) = \frac{1}{2}\int_\Omega |\nabla f|^2,$$

where the gradient operator ∇ and the norm are taken with respect to the standard metrics in $\mathbf{R}^2$ and $\mathbf{R}^n$, respectively. (In coordinates, $|\nabla f|^2 = \mathrm{tr}({}^t\partial f\, \partial f)$, where ∂f is the matrix of partial derivatives of f in an orthonormal basis.) This drastically reduced the scope of the problem from the class of all parametrizations to the class of all conformal parametrizations.

From the numerical point of view there exist a number of methods to compute minimal surfaces: see, for example, [Wilson 1961, Concus 1967, Wohlrab 1985, Sullivan 1990, Dziuk 1991, Brakke 1992]. In this paper we present a new algorithm that splits the minimization process into a sequence of steps that involve computing harmonic maps on surfaces, without reference to any two-dimensional parameter domain. We also minimize with respect to variations of boundary points lying on straight boundary lines, and of points lying on free boundary curves restricted to planes. Therefore the resulting discrete minimal surfaces may be extended across boundary symmetry lines as discrete minimal surfaces.

We also present for discrete harmonic maps an algorithm computing a conjugate harmonic map (Section 5), which, as far as we know, is the only method that gives reasonable results. Instead of trying to simulate the continuous case, we use the discrete data of our minimization process directly to compute a discrete conjugate surface. Therefore, there is no loss of accuracy during the conjugation process. Additionally, our conjugation process respects symmetries of the discrete surfaces: if the image of a harmonic map has symmetry lines, the conjugate image will have the corresponding symmetry properties (Section 2). Since for a minimal surface the identity map is harmonic, we can compute the conjugate minimal surface using the same algorithm.

We mention in more detail two major approaches for computing minimal surfaces, since our minimization algorithm is in some sense a mixture of both.

The first approach has its origin in the theoretical existence proofs of Douglas and Radó, as later reformulated by Courant, and tries to imitate them numerically. It works with discrete surfaces parametrized over the triangulated unit disk B. For a given curve $\Gamma \subset \mathbf{R}^3$, one starts with an initial parametrization $f : B \to \mathbf{R}^3$ with $f(\partial B) = \Gamma$, and successively repeats a two-part minimization step:

- minimize the Dirichlet energy $E_D(f)$ by varying points in image space, and
- minimize $E_D(f)$ by varying points of the discretization in the planar domain B.

We will call the first step the *Dirichlet step* and the second the *conformal step*, since it is used to make the map f conformal: see Section 2 for more details. During the Dirichlet step a fixed parameter domain is assumed. The numerical minimization of the Dirichlet integral is then a linear problem, and is straightforward. But for the conformal step the different algorithms vary; see [Wohlrab 1985] and [Hutchinson 1991], for example.

Varying points in the domain may be interpreted as varying the metric to make the map conformal. In the continuous case this would be accomplished by taking the induced metric, and the map would be immediately an isometry and therefore conformal. In the discrete case even defining conformality presents a problem. For example, it is usually not possible to get a conformal map in the sense that angles in corresponding domain and image triangles are the same, since the domain is flat. The best one can do is minimize the so-called *conformal energy* $E_D(f) - A(f)$, but without hope of getting it to vanish.

The second major approach to computing minimal surfaces is via mean curvature flow. Numerically this is the most natural approach, since the area is directly minimized by letting the surface flow in the normal direction, with speed equal to

the mean curvature. This is equivalent to moving along the direction of the area gradient in the space of surfaces. In contrast with the former approach, here everything happens in image space, without the need for a two-dimensional parameter domain. Two drawbacks of this approach are that boundary points may only vary orthogonally to the curve, and that singularities develop in general at thin necks, even if the boundary curve is planar. For implementations of algorithms based on this idea, see [Dziuk 1991] and [Brakke 1992].

Our minimization algorithm combines aspects of both methods. It uses as the fundamental minimization step the Dirichlet step from the first algorithm, with the following modification: for a given boundary Γ and metrical surface M_i we compute the next surface M_{i+1} as the minimizer of the Dirichlet functional

$$M_{i+1} := \min_M \frac{1}{2} \int_{M_i} |\nabla(f : M_i \to M)|^2.$$

Note that we do not use a planar two-dimensional domain, but instead the most recently computed surface M_i. Such a trick was also applied in computing the mean curvature flow in [Dziuk 1991] to mitigate numerical difficulties with the Laplace operator.

Numerically we are left within each step with a linear problem of computing the surface M_{i+1} where the minimum of the quadratic function is attained. This new minimization method is faster than in the first algorithm, since the nonlinear conformal step is completely skipped. It is no longer necessary to adapt the conformal structure of the parameter domain because at each step we start with the conformal identity map. This also avoids numerical inaccuracies arising from inaccurate conformal structures in the domain.

Since we always step to the absolute minimum of the Dirichlet integral in each iteration, and since we do not move along the area gradient, we proceed discretely also in the time direction. Compared to the mean curvature flow we therefore have fewer problems with singularities of mean curvature type arising, for example, at thin handles (see Figure 12), and we have more flexibility in moving points tangentially to the boundary. Our algorithm also handles situations where lines are shared by multiple surfaces (see Figure 18). Figures 10–20 at the end of this article illustrate several surfaces generated by the algorithm.

The algorithms and the graphics output were implemented using the mathematical programming environment Grape. (Grape is an object-oriented graphics system with special applications to problems from differential geometry and continuum mechanics, developed at the Sonderforschungsbereich 256 at the University of Bonn, from which it may be obtained on request: see the second author's address.)

2. GENERAL SETUP

Before starting with the discrete case, we review a few definitions and results from the continuous case.

Let $\Gamma = \{\Gamma_1, \ldots, \Gamma_n\}$ be a collection of simple closed curves and M a surface with boundary $\partial M = \Gamma$.

Definition 1. M is a *minimal surface* if and only if for each point $p \in M$ one can choose a small neighborhood $U(p)$ that has minimal area among other patches V having the same boundary as U.

By this definition, minimal surfaces are characterized by having locally least area compared to small variations of the surface.

Let (N, g) and (M, h) be Riemannian manifolds with metrics g and h, and let $f : \Omega \subset N \to M$ be a parametrization of a surface $f(\Omega) \subset M$ over a two-dimensional domain submanifold $\Omega \subset N$. Then the *area* of $f(\Omega)$ is given by

$$A(f) = \int_\Omega \text{Jacobian}(f)$$

and the *Dirichlet energy* of the map f is defined as

$$E_D(f) = \frac{1}{2} \int_\Omega |\nabla_g f|_h^2,$$

where ∇_g is the gradient operator with respect to the metric g and $|\cdot|_h$ is the norm in image space with respect to the metric h. (In coordinates, we have $|\nabla_g f|_h^2 = \mathrm{tr}({}^t\partial f\, \partial f)$, where ∂f is the matrix of partial derivatives expressed in bases orthonormal with respect to g and h.) We will use the subscripts g and h as need, to indicate the metric under consideration.

It is well known that $A(f(M)) \leq E_D(f)$, with equality if and only if f is a conformal map. Following [Hutchinson 1991] we will call the difference

$$E_C(f) = E_D(f) - A(f(M)) \qquad (2.1)$$

the *conformal energy* of the map f. This is justified by the observation that for Euclidean (x, y)-domains the quantity

$$E_C(f) = \frac{1}{2}\int_\Omega |D^{\pi/2} f_x - f_y|^2,$$

where $D^{\pi/2}$ is the 90° rotation in the oriented tangent plane, is a natural measure of a map's deviation from conformality.

Let M be a three-dimensional space form (that is, a complete three-manifold of constant curvature). Minimal surfaces in M come in families. More precisely, let $f : \Omega \to M$ be a minimal immersion of a simply connected domain Ω. Then f has an *associated family*

$$f^\theta : \Omega \to M$$

of isometric minimal immersions, defined as follows: Associate with f the data (g, S), where g is the metric induced by f on Ω, and S is the Weingarten map, defined by $\nabla f \cdot S = \nabla N$ with N the normal map of the surface. The maps f^θ are those whose associated geometric data (g^θ, S^θ) are given by

$$g^\theta := g, \qquad S^\theta := D^\theta S, \qquad (2.2)$$

where D^θ is the rotation about the angle θ in the oriented tangent planes of Ω. We call $f^{\pi/2}$ the *conjugate immersion* of f. The maps f^θ are determined up to isometries of M by these conditions. See [Lawson 1970] for more details.

Minimal surfaces in M have useful symmetry properties. If a minimal surface contains a straight line (geodesic) of M, it is invariant under a 180° rotation around this line. A minimal surface that meets a totally geodesic plane in M orthogonally along an arc is invariant under reflection in this plane. These properties allow the construction of complete surfaces from fundamental pieces that are bounded by symmetry lines.

The symmetry properties are also an essential tool for the existence proof called *conjugate surface construction*. This construction, originally invented by Smyth [1984] to prove the existence of three minimal patches in a given Euclidean tetrahedron, is based on the fact that a straight line on a minimal surface corresponds to a planar line of symmetry on the conjugate surface, and vice versa. A minimal surface that is cut by its symmetry planes into simply connected domains has therefore a conjugate domain bounded by straight lines. To prove the existence of the original piece one can often reconstruct the conjugate polygonal contour using only knowledge about the symmetry planes. Then the Morrey solution (for example) to the Plateau problem for the polygonal contour proves the existence of the conjugate patch and, by conjugation, also of the desired patch bounded by symmetry planes. See [Karcher 1989] for conjugate constructions in $\mathbf{R}^3$, [Karcher et al. 1988] in $\mathbf{S}^3$ and [Polthier 1991] in $\mathbf{H}^3$.

3. DISCRETE MINIMAL SURFACES

In this section we define discrete surfaces and other analogs of terms known from the continuous case. We will see especially that the energy of a discrete map and its derivative can be expressed in geometric terms.

Definition 2. A *discrete surface* in a three-dimensional space form is a topological simplicial complex consisting of triangles. The triangles may degenerate to lines or points.

Definition 3. A *discrete minimal surface* is a discrete surface such that small perturbations of vertices do not decrease the total area.

In the following we assume that each discrete surface lies in a vector space endowed with a constant metric. Let T_1 and T_2 be two triangulations in vector spaces, i.e., two discrete surfaces in the sense of Definition 2, with induced metrics g and h. If the abstract simplicial complexes of T_1 and T_2 are identical, we can define a simplicial map

$$f : (T_1, g) \to (T_2, h)$$

between the two triangulations by mapping each vertex of T_1 to the corresponding vertex on T_2, and extending f linearly (affinely) to each triangle. The metric on each triangle of T_1 and T_2 is induced by the metric of the ambient vector space.

Definition 4. The *energy* of a simplicial map between discrete surfaces is the sum of the energies of the restrictions

$$f_i : (\Delta_{1,i}, g) \to (\Delta_{2,i}, h),$$

where $\Delta_{1,i}$ and $\Delta_{2,i}$ are corresponding triangles in T_1 and T_2, and the energies of the atomic maps f_i are defined as in the continuous case. More precisely, the energy $E_D(f_i)$ of the atomic linear map f_i is

$$E_D(f_i) = \frac{1}{2} \int_{(\Delta_i, g)} |\nabla_g f_i|_h^2,$$

with the same notation as in Section 2 (see top of page 18).

It turns out that for a linear map $f : \Delta_1 \to \Delta_2$ between triangles Δ_1 and Δ_2 there is an explicit representation of $E_D(f)$ in terms of the angles (the "conformal structure") of Δ_1 and the side lengths of Δ_2:

Lemma 5. *Let f be a linear map between two triangles Δ_g and Δ_h in two vector spaces with constant metrics g and h. Then the Dirichlet energy of f is*

$$E_D(f) = \tfrac{1}{4}(\cot\alpha\,|a|_h^2 + \cot\beta\,|b|_h^2 + \cot\gamma\,|c|_h^2),$$

where α, β, γ are the angles of Δ_g with respect to the metric g, and $|a|_h$, $|b|_h$, $|c|_h$ are the corresponding side lengths of Δ_h with respect to the metric h.

Proof. Let the linear map be defined by $f(v) = a$ and $f(w) = b$ (see Figure 1 for the notation). Let $\{e_1, e_2\}$ be the canonical basis of $\mathbf{R}^2$ and Δ_e the triangle built thereon. Then we can write $f = \psi \circ \varphi^{-1}$, where $\varphi : \Delta_e \to \Delta_g$ and $\psi : \Delta_e \to \Delta_h$ are the linear maps taking $\{e_1, e_2\}$ to $\{v, w\}$ and $\{a, b\}$, respectively.

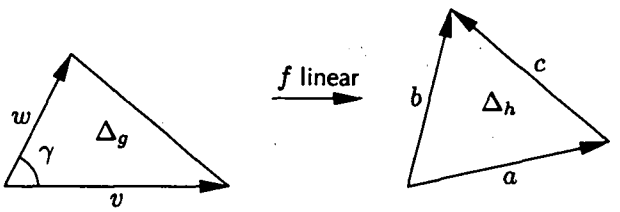

FIGURE 1. Atomic linear map between two triangles

In the rest of this proof we omit the subscript indicating the metric with respect to which scalar products and norms are taken.

Denoting by ∂f, $\partial\varphi$ and $\partial\psi$ the matrices of partial derivatives with respect to $\{e_1, e_2\}$ in the domain and arbitrary orthonormal bases in the range, we have

$${}^t\partial\psi\,\partial\psi = \begin{pmatrix} \langle a,a\rangle & \langle a,b\rangle \\ \langle a,b\rangle & \langle b,b\rangle \end{pmatrix}$$

and

$$\partial\varphi^{-1}\,{}^t\partial\varphi^{-1} = \frac{1}{D^2}\begin{pmatrix} \langle w,w\rangle & -\langle v,w\rangle \\ -\langle v,w\rangle & \langle v,v\rangle \end{pmatrix},$$

where $D := \det\partial\varphi$. We also have $\partial f = \partial\psi\,\partial\varphi^{-1}$. Therefore

$$\begin{aligned} \operatorname{tr}({}^t\partial f\,\partial f) &= \operatorname{tr}({}^t\partial\varphi^{-1}\,{}^t\partial\psi\,\partial\psi\,\partial\varphi^{-1}) \\ &= \operatorname{tr}({}^t\partial\psi\,\partial\psi\,\partial\varphi^{-1}\,{}^t\partial\varphi^{-1}) \\ &= D^{-2}\big(\langle a,a\rangle\langle w,w\rangle \\ &\qquad - 2\langle a,b\rangle\langle v,w\rangle + \langle v,v\rangle\langle b,b\rangle\big). \end{aligned}$$

Now $c = b - a$, so $-2\langle a,b\rangle = |c|^2 - |a|^2 - |b|^2$, and we get successively for $\operatorname{tr}({}^t\partial f\,\partial f)$:

$$D^{-2}((\langle w,w\rangle - \langle v,w\rangle)|a|^2 + (\langle v,v\rangle - \langle v,w\rangle)|b|^2 + \langle v,w\rangle|c|^2)$$
$$= D^{-2}(\langle -w, v-w\rangle|a|^2 + \langle w-v, -v\rangle|b|^2 + \langle v,w\rangle|c|^2)$$
$$= D^{-1}(\cot\alpha\,|a|^2 + \cot\beta\,|b|^2 + \cot\gamma\,|c|^2).$$

In the last step we used the identities

$$\cos\gamma = \frac{\langle v,w\rangle}{|v|\,|w|}, \quad \sin\gamma = \frac{D}{|v|\,|w|},$$

and correspondingly for α and β.

The Dirichlet energy is then

$$E_D(f) = \frac{1}{2}\int_{\Delta_g} |\nabla f|^2 r = \operatorname{tr}({}^t\partial f\,\partial f)$$
$$= \frac{1}{2}\int_{\Delta_e} \operatorname{tr}({}^t\partial f\,\partial f)\det\partial\varphi^{-1}$$
$$= \tfrac{1}{4}(\cot\alpha\,|a|^2 + \cot\beta\,|b|^2 + \cot\gamma\,|c|^2),$$

the additional factor $\frac{1}{2}$ being the area of Δ_e. □

This representation is so natural that it should have appeared somewhere in the literature, but we have not found it. Compare Wilson [1951] for a different and less clear examination of the triangular Dirichlet energy. Our representation immediately shows the conformal invariance of the Dirichlet energy with respect to conformal changes of the domain metric, and the quadratic dependence on the side lengths in image space.

As an immediate consequence we can now define the Dirichlet energy of a map f between two discrete surfaces as the sum of all energies on triangles:

$$E_D(f) = \sum_{\text{triangles } i} E_D(f_i)$$
$$= \tfrac{1}{4}\sum_{\text{edges } i} (\cot\alpha_i + \cot\beta_i)|a_i|^2. \qquad (3.1)$$

In the last representation we merged the two terms corresponding to each edge; α_i and β_i are the angles opposite to a_i in the two adjacent triangles. For boundary edges one term is taken to be zero. Heuristically the representation may be considered as the weighted sum of all edge lengths, where the weights depend only on the domain. In this interpretation the energy is concentrated on the edges as tension; but note that the tension may be negative, meaning that the edge acts with a repelling force on its end points.

We will prove some further useful identities for planar triangles. In the notation of Figure 2, we

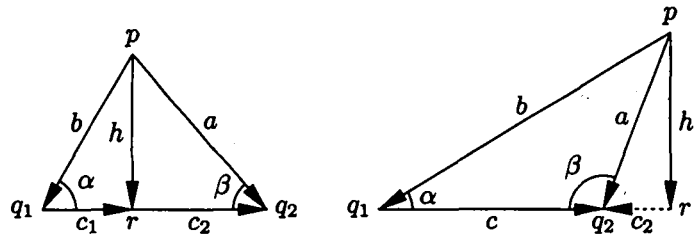

FIGURE 2. Notation for triangles. In both cases we let r be the orthogonal projection of p on the opposite side, and set $c_1 = r - q_1$, $c_2 = r - q_2$ and $c = c_1 + c_2 = q_2 - q_1$.

have $\cot\alpha\,h = -D^{\pi/2}c_1$, $\cot\beta\,h = -D^{\pi/2}c_2$, and $a = h + c_2$, $b = h - c_1$. It follows immediately that $\cot\alpha + \cot\beta = |c|/|h|$, and further that

$$\cot\alpha\,a + \cot\beta\,b = -D^{\pi/2}c.$$

Computing formally the energy for the identity map on a triangle Δ with angles α, β, γ and sides a, b, c, we obtain twice the area:

$$\tfrac{1}{2}(\cot\alpha\,|a|^2 + \cot\beta\,|b|^2 + \cot\gamma\,|c|^2) = 2\ \text{area}\,\Delta.$$

We are now ready to define a discrete harmonic map, by analogy with the continuous case:

Definition 6. A *discrete harmonic map* is a critical point for the Dirichlet energy functional with respect to variations of interior surface vertices in image space. To take into account symmetry properties we also allow boundary points to vary in some cases:

- If an arc in the domain boundary is straight, and likewise its image, it is a line of symmetry and the interior points of the image boundary arc may vary along the line.
- If an arc in the domain boundary lies in a plane, and is a symmetry curve, the interior points

of the image boundary may vary in the image plane. (This allows the modeling of free boundary problems.)

In all other cases the image boundary points remain fixed.

The condition for local harmonicity is explicitly given by differentiating expression (3.1):

$$\frac{\partial}{\partial p} E_D(f) = \tfrac{1}{2} \sum_{\substack{\text{vertices } q_i \\ \text{adjacent to } p}} (\cot \alpha_i + \cot \beta_i)(p - q_i) = 0, \tag{3.2}$$

or, equivalently,

$$p = \frac{\sum_i (\cot \alpha_i + \cot \beta_i) q_i}{\sum_i \cot \alpha_i + \cot \beta_i}.$$

If this condition is true for all interior points p, then f is a critical point for the discrete energy functional. The condition for points on boundary symmetry lines is the same except that the full vertex star around a point p has to be constructed according to the symmetry properties.

We will now have a closer look at the numerical procedure to compute a harmonic map. For simplicity we do not allow boundary points to move in the following, i.e., we assume we have a Dirichlet problem: given a triangulated domain Ω and a map $f : \partial\Omega \to \Gamma$, where Γ is a fixed polygonal contour, we seek a harmonic extension of f to the interior of Ω. In general, if the problem involves symmetries (Definition 6), the corresponding boundary points are allowed to move, subject to the relevant boundary conditions.

Remarks. (a) In the continuous case the extension is unique in Euclidean space.

(b) In practice our algorithm uses $\partial\Omega = \Gamma$.

Let the triangulation have I interior vertices and B boundary vertices, and let $P = (p_1, \ldots, p_{B+I})$ be a representation of $f(\Omega)$, the p_i being interior vertices for $i > B$ and boundary vertices for $i \leq B$. Minimizing $E_D(f)$ is a quadratic problem and has a unique solution. We therefore write it using a quadratic form:

$$\begin{aligned} E_D(f) &= \tfrac{1}{4} \sum_{\text{edges } i} (\cot \alpha_i + \cot \beta_i) |a_i|^2 \\ &= \tfrac{1}{8} \sum_{\substack{\text{pairs } (i,j) \\ \text{of adjacent vertices}}} (\cot \alpha_{ij} + \cot \beta_{ij}) |p_i - p_j|^2 \\ &= P^t S P, \end{aligned}$$

where S, analogous to the well-known stiffness matrix from finite element theory, has the following entries (where $i \neq j$ and id is the identity map on the ambient vector space):

$$S_{ij} = \begin{cases} -\frac{1}{8}(\cot \alpha_{ij} + \cot \beta_{ij})\mathrm{id} & \text{for } p_i, p_j \text{ adjacent,} \\ 0 & \text{otherwise,} \end{cases}$$

$$S_{ii} = \sum_{\substack{p_j \text{ adjacent} \\ \text{to } p_i}} -S_{ij}.$$

S is symmetric, and is positive definite on all triangulations P having positive area: indeed, we have ${}^tPSP = E_D(f) \geq \operatorname{area} P > 0$.

The condition for a surface to attain the minimum of the Dirichlet energy while keeping the boundary points fixed is as follows: Let

$$X = (p_1, \ldots, p_B, x_{B+1}, \ldots, x_{B+I})$$

be an admissible surface with fixed boundary points p_i and free interior points x_i, and let

$$\tilde{X} = (0, \ldots, 0, x_{B+1}, \ldots, x_{B+I})$$

be an admissible variation direction. Then

$$\begin{aligned} 0 = \frac{\partial E_D(f)}{\partial \tilde{X}}\bigg|_{X=P} &= \frac{\partial (X^t S X)}{\partial \tilde{X}}\bigg|_{X=P} \\ &= 2(0, \ldots, 0, \mathrm{id}, \ldots, \mathrm{id})\, SX. \end{aligned}$$

We denote this last matrix by Q, with entries

$$Q_i = \begin{cases} 0 & \text{if } i \leq B, \\ 2\left(\sum_{j=1}^{B} S_{ij} p_j + \sum_{j=B+1}^{B+I} S_{ij} x_j\right) & \text{if } i > B. \end{cases}$$

Thus the interior points x_i can be computed by solving the linear system of equations $Q_i = 0$, for $B < i \leq B + I$.

Smooth harmonic maps defined on a planar domain are characterized by their mean value property: the center of a small circle is mapped to the center of mass of the circle's image. This has the consequence that the image of a harmonic map lies inside the convex hull of its boundary. For discrete harmonic maps a corresponding mean value property follows immediately from the local harmonicity condition (3.2) [Wilson 1961]:

Lemma 7. *Let f be a discrete harmonic map defined on the points $\{q_i\}$ around a point p. If the points $\{q_i\}$ form a regular planar polyhedron with center p, then $f(p)$ is the center of mass of the $\{f(q_i)\}$.*

But this result does not hold in general for other planar or spatial domains. Nevertheless we have a convex hull property for discrete harmonic maps as long as the spatial domain consists only of acute triangles.

Lemma 8. *Let f be a discrete harmonic map defined on a spatial domain formed by the points $\{q_i\}$ around a point p. If the triangles around p are all acute, then $f(p)$ lies in the convex hull of $\{f(q_i)\}$.*

Proof. From the local harmonicity condition (3.2) we see that p can be represented as a linear combination of the points $\{q_i\}$. Since all angles are acute, the weights of the q_i are in the interval $(0, 1)$, so p is a convex combination. □

Lemma 9. *Discrete minimal surfaces have the convex hull property, since they are critical points of the area functional.*

4. THE MINIMIZATION ALGORITHM

In Section 3 we explained a method to compute a discrete harmonic map for a given triangulated domain and a given boundary configuration Γ in image space. We allowed Γ to consist of a collection of curves, each marked as being a fixed curve, a symmetry straight line or a planar symmetry arc; when there are symmetry lines or arcs the boundary points thereon are allowed to vary, as stated in Definition 6.

We call two collections Γ and Γ' equivalent, and write $\Gamma \sim \Gamma'$, if the vertices of Γ and Γ' are identical along fixed arcs and are in one-to-one correspondence along each symmetry line and each planar symmetry arc.

Our algorithm attacks the following problem:

Problem. Given a boundary configuration Γ and an initial discrete surface M_0 with $\partial M_0 \sim \Gamma$, find a locally area-minimizing discrete surface M in the class $\mathbf{M}$ of all discrete surfaces with simplicial complex homeomorphic to that of M_0, with boundary equivalent to Γ, and that can be extended across symmetry lines and arcs of ∂M as a local minimizer.

To simplify the description of the algorithm, we have formulated the problem in a very restrictive way; for example, we do not allow adaptive changes of the triangulation and topology changes for the moment. Section 6 contains a discussion of topology changes. (Our implementation uses an adaptive refinement procedure depending on discrete curvature, which we will not discuss in this paper; but see Figure 16.)

Algorithm. 1. Take the initial surface M_0 as the first approximation of M; set i to 0.

2. Compute the next surface M_{i+1} as the minimum of the Dirichlet energy

$$F_i(X) := E_D(f : M_i \to X)$$

among all permissible data $f : M_i \to X$. This is a linear problem. The condition for the minimum is given by (3.2).

3. Set i to $i + 1$ and repeat Step 2.

In practice, we use the termination criterion

$$|\text{area}\, M_i - \text{area}\, M_{i+1}| < \varepsilon.$$

Proposition 10. *The algorithm converges to a solution of the problem if no triangles degenerate.*

Proof. Saying that no triangles degenerate means, by definition, that the angles of all the triangles in all the M_i are uniformly bounded away from 0

and π. Thus we are dealing with a compact set of surfaces. From the construction, the areas of the M_i and the energies of the minimizing maps $f_i : M_i \to M_{i+1}$ are monotonically decreasing:

$$\begin{aligned}\operatorname{area} M_i &= E_D(\mathrm{id}|_{M_i}) \\ &\geq E_D(f_i) = \operatorname{area} M_{i+1} + E_C(f_i) \\ &\geq E_D(\mathrm{id}|_{M_{i+1}}) = \operatorname{area} M_{i+1}.\end{aligned}$$

Therefore a subsequence of the M_i converges uniformly to a limit surface M, that is, $|M_i - M| \to 0$. (Here the norm may be taken, for instance, as the maximum distance between corresponding vertices.) We must show that M is minimal. Now F_i, the Dirichlet energy function for maps $f : M_i \to X$, is a quadratic function with minimum at M_{i+1}: in symbols,

$$\nabla F_i|_{M_{i+1}} = 0.$$

Because of the nondegeneracy condition we have a uniform bound $s_{\max}$ on the norm of $\nabla^2 F_i$, independent of i. Using the mean-value theorem we can write

$$\nabla F_i|_{M_i} = \nabla F_i|_{M_i} - \nabla F_i|_{M_{i+1}} = \nabla^2 F_i|_\xi \, (M_i - M_{i+1})$$

for some $\xi \in \mathbf{M}$, so that

$$\left|\nabla F_i|_{M_i}\right| \leq s_{\max} |M_i - M_{i+1}|.$$

Since $M_i \to M$ it follows that

$$\nabla F_i|_{M_i} \to \nabla F_M|_M = 0,$$

where F_M is the Dirichlet energy function for maps $f : M \to X$. Thus M is a critical point for F_M, and so also for the area functional. □

The nondegeneracy condition is in general not a priori verifiable. See, for example, Figures 13–15, where no minimizer in the class of triangulations with the same topology as the initial triangulations exist.

Our algorithm is different from the mean curvature flow algorithm and may lead to different results. For example, consider the initial triangulation in Figure 12. Mean curvature flow type algorithms would lead to a singularity at the small waist. Our algorithm proceeds discretely also in time direction; in this example it reaches a minimal configuration in one minimization step, and without passing through a singular situation.

5. THE CONJUGATION ALGORITHM

One of the main problems that conjugation algorithms have to deal with is the need to use inaccurate discrete data out of a minimization process as an approximation to a smooth surface, since all known approaches try to simulate the procedure implicit in (2.2) for the smooth case.

The advantage of our method for discrete minimal surfaces—which, as far as we know, is the only method that gives reasonable results—is that we use the discrete data of the minimization process directly to compute a discrete conjugate surface. As we will see (Theorem 11), the discrete minimality condition (3.2) is simultaneously the integrability condition for the discrete conjugate surface, which means that we lose no accuracy during the conjugation process.

The algorithm is defined for a triangular graph M that is a critical point for the area functional, but it may also be applied to harmonic maps between two discrete surfaces. M may have been obtained, for example, by the minimization procedure described in the previous sections. For each vertex p, the minimality condition

$$\frac{1}{2} \sum_{\substack{\text{vertices } q_i \\ \text{adjacent to } p}} (\cot \alpha_i + \cot \beta_i)(p - q_i) = 0$$

means geometrically that the weighted edges emanating from p add up to zero, and so can be arranged as a closed polygon. This closed polygon is defined as the dual cell of the point p. This works perfectly for interior points. For points along the boundary we distinguish two cases:

- If the point belongs to a planar or straight symmetry arc, the whole neighborhood is uniquely determined by the symmetry properties, and the algorithm works as for interior points.

- If a point p is not on a symmetry arc, the construction of a neighborhood is usually not possible. We then assume the existence of a neighborhood such that all weighted edges add up to zero. It is of no further relevance how this strip around the boundary curve is defined, since the conjugation algorithm only requires knowledge of the two boundary vertices adjacent to p and of an edge from p into the interior.

So, how does the conjugation process work? Consider a neighborhood of a point p on the discrete minimal surface, as in Figure 3. The identity map f

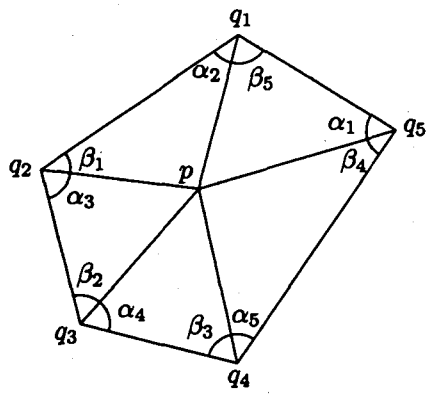

FIGURE 3. Neighborhood around a point

from the discrete surface to itself is a discrete harmonic map by assumption. Its restriction to a single triangle is a smooth linear map. Conjugation in the smooth case means rotating the one-form df of the map f in each tangent space. Here this operation is only defined on the smooth linear triangles, but along the edges it results in discontinuities of the atomic one-forms. In spite of these discontinuities, we can give a definition that makes sense.

We define a global star operator acting on the differential df of f by

$$*df := df \cdot J,$$

where J is the well-defined 90° rotation on the interior of each triangle. The form $*df$ is not closed globally, but it turns out that it can be integrated along very special paths. Consider two adjacent

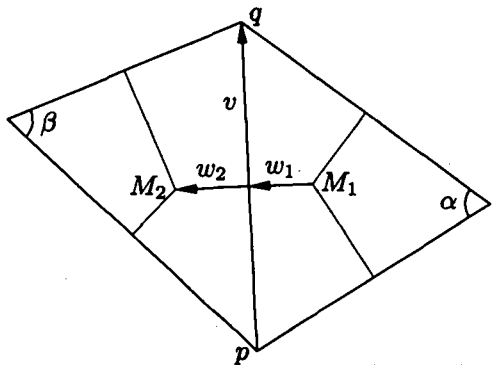

FIGURE 4. Path between two adjacent triangles. M_1 and M_2 are the centers of the triangle's circumcircles, while w_1 and w_2 lie along the perpendicular bisector of edge pq.

triangles, not necessarily coplanar, as in Figure 4. An elementary calculation shows that

$$w_1 = \cot\alpha\, Jv, \quad w_2 = \cot\beta\, Jv,$$

where J is taken with respect to the appropriate triangle, and further that

$$*df(w_1) = -\cot\alpha\, v, \quad *df(w_2) = -\cot\beta\, v.$$

This means that $*df$ is continuous across triangle edges when applied to vectors orthogonal to the edges.

We now integrate the one-form $*df$ along the path γ formed by the perpendicular bisectors of the edges incident on p. This is equivalent to adding up the corresponding weighted vectors. Now we arrived at the most important point: the resulting expression vanishes,

$$\int_\gamma *df = -\sum_{\text{neighbors of } p} (\cot\alpha_i + \cot\beta_i)v_i = 0,$$

precisely because the initial triangulation satisfies the minimality condition (3.2). Thus:

Theorem 11. *The closedness condition for the dual one-form $*df$ is equivalent to the minimality condition for the initial triangulation f.*

Since $*df$ is closed along the path formed by the perpendicular bisectors, we obtain a dual cell for

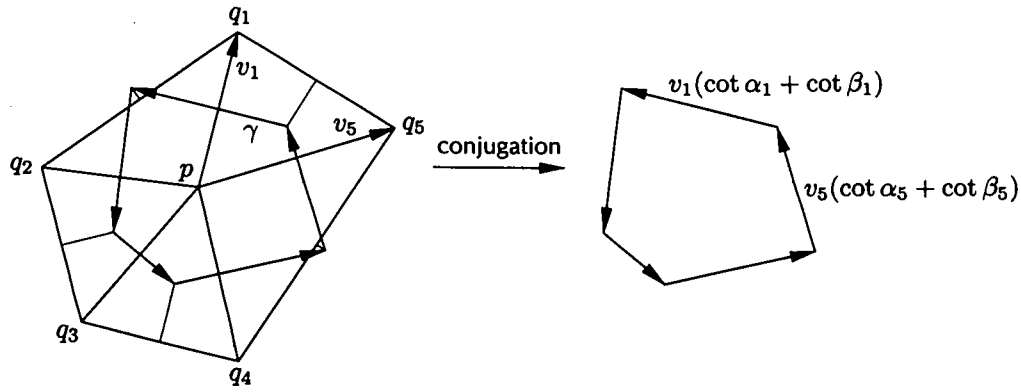

FIGURE 5. Action of conjugation on the star of a vertex. Integrating the atomic one form $*df$ along the path γ consisting of all mid perpendiculars around a vertex p gives cell dual to p in the conjugate triangulation. For clarity, we have rotated the right-hand side by $-90°$.

each vertex p, as in Figure 5. Continuing we get a well-defined dual graph to the given minimizing triangulation. To each triangle of the original triangulation there is an associated vertex of the dual graph, with three adjacent vertices. Every such set of four vertices lies in a plane, since the three edges of the triangle are coplanar.

We are further interested in finding a triangulation of the dual surface that has the same underlying simplicial complex as the original triangulation, because then the associated family of the minimizing triangulation is also defined. As remarked above, this same-topology triangulation cannot be canonically defined since the one-form $*df$ is not globally closed. But we can still integrate the form canonically in the interior of each triangle. This gives a dual complex of triangles that match at the common base points of their perpendicular bisectors. A good approximation now for the center of each dual cell is the mean of all triangle vertices lying inside the dual cell (Figure 6).

In the case of a vertex q lying on a fixed boundary arc, a whole neighborhood is usually not constructible. To conjugate such points we use information available from the dual cell of an adjacent interior point. Look at Figure 6 and assume q_i lies on a fixed boundary arc, p being an adjacent interior point. By conjugating a neighborhood of p, we automatically obtain $f_i^*(q_i)$, which is an ideal candidate for the dual point of q_i. Compared to the conjugation of interior points, this method differs only in that a final averaging is not possible.

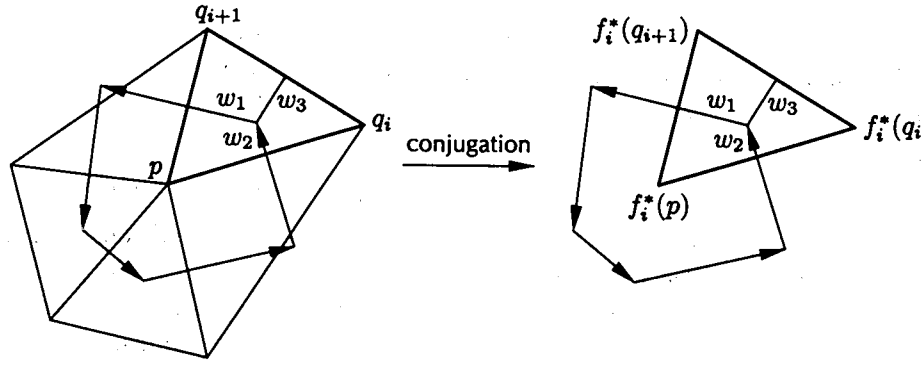

FIGURE 6. Action of conjugation on a cell. Integrating the atomic one form $*df$ inside the triangle (p, q_i, q_{i+1}) leads to a well-defined triangle, whose perpendicular bisectors are part of the dual graph. The image $f^*(p)$ is defined as the mean of the $f_i^*(p)$.

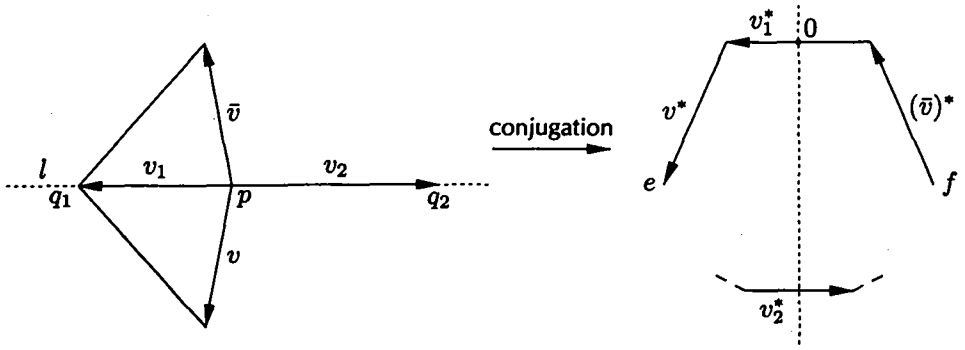

FIGURE 7. A straight line in the original surface gives a planar symmetry curve in the conjugate.

In the continuous case, the conjugate of a planar surface is the same surface rotated by 90°. We now prove that applying our conjugation algorithm to a discrete planar surface also gives a rotated copy.

Lemma 12. *For a planar initial triangulation, the algorithm just described yields exactly the conjugate minimal surface.*

Proof. In the planar case the operator J is constant on the triangulation. Therefore $*df$ is globally closed on the triangulation T, and is the differential of

$$f^* = -Jf : T \to T^*,$$

which maps T to its conjugate triangulation T^*, namely, T rotated by 90° □

Here is a further property of the discrete conjugation method:

Lemma 13. *Straight lines of a minimizing triangulation are mapped to planar symmetry curves of the conjugate triangulation. Conversely, planar symmetry curves are taken to straight lines.*

Proof. Let p be a boundary point lying in the interior of a straight line l, and having as neighbors along the boundary q_1 and q_2. The vertex star of p consists of q_1 and q_2, plus points in the interior of the surface and their reflected images: see Figure 7.

To construct the dual cell, we add the weighted edges emanating from p in a circular sequence. Let v be a vector emanating from p. It can be written as the sum of a component parallel to l and one orthogonal:

$$v = v_l + v_l^{\perp},$$

The vector $\bar{v}$ symmetric to v with respect to l equals

$$\bar{v} = v_l - v_l^{\perp}.$$

We now start building the dual cell with the vector v_1^* parallel to l. Without loss of generality we can place the midpoint of v_1^* at the origin. At the tip of v_1^* we place the base of the next vector v^*, and at base of v_1^* we place the tip of $\bar{v}^*$. The two endpoint of the polygonal lines, denoted e and f in Figure 7, can thus be written

$$e = \tfrac{1}{2}v_1^* + v_l + v_l^{\perp},$$
$$f = -\tfrac{1}{2}v_1^* - v_l + v_l^{\perp}.$$

It follows by induction that the dual cell is symmetric with respect to the plane orthogonal to l and going through the center of v_1^* and v_2^*.

In the same manner one proves that planar symmetry lines are mapped to straight lines in the conjugate surface. □

6. TOPOLOGY CHANGES

In this section we discuss ongoing experiments with changes in the topology (connectivity) of a discrete surface during the minimization process. The aim of these experiments is to be able to compute beyond singular situations, when the triangulation becomes degenerate, and thereby compactify the class of discrete surfaces occurring during

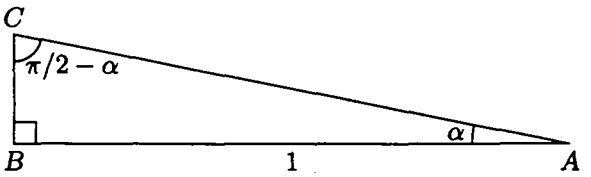

FIGURE 8. A triangle about to degenerate.

the minimization process. "Degenerate triangulation" means that triangle angles become 0 or π. This happens when a triangle's vertices become collinear, or when two or three vertices merge into a point. From the theoretical point of view these situations are not dangerous, since the energy and its derivative of a map taking such a degenerate triangle to a non-degenerate one would be infinite. Thus the triangle would remain unchanged when continuing the iteration. The problems that might occur are purely numerical.

But it turns out that one can go around these difficulties with a more careful analysis. We consider the case where a vertex falls onto the opposite edge as a special case of the situation where two points merge, by dividing the triangle along the short altitude and applying the analysis separately to the two resulting right triangles.

Let A, B, C be the vertices of a right triangle (Figure 8), where the length $\overline{BA}$ is normalized to one. Consider how the energy changes as C varies, for α small. The energy is

$$E = \tfrac{1}{4}(\cot\alpha\,|B-C|^2 + \cot(\pi/2-\alpha)),$$

so

$$\frac{\partial E}{\partial C} = \tfrac{1}{2}\cot\alpha\,(C-B) = \frac{C-B}{2\,|C-B|}$$

$$\frac{\partial^2 E}{\partial C^2} = \tfrac{1}{2}\cot\alpha\,\mathrm{id}.$$

We conclude that moving C a little bit while α is very small would cost a very large amount of energy. So once a triangle degenerates, it remains degenerate during further minimizations. The consequence for the numerical algorithm is that we can compute beyond singular situations: once such a situation occurs we can simply remove the singular triangle using the rules shown in Figure 9. The total number of triangles is less or equal than before.

ACKNOWLEDGEMENTS

This work was done while the second author visited the Sonderforschungsbereich 288 in Berlin. He thanks the SFB for the hospitality he enjoyed.

The authors would like to thank U. Brehm for fruitful discussions.

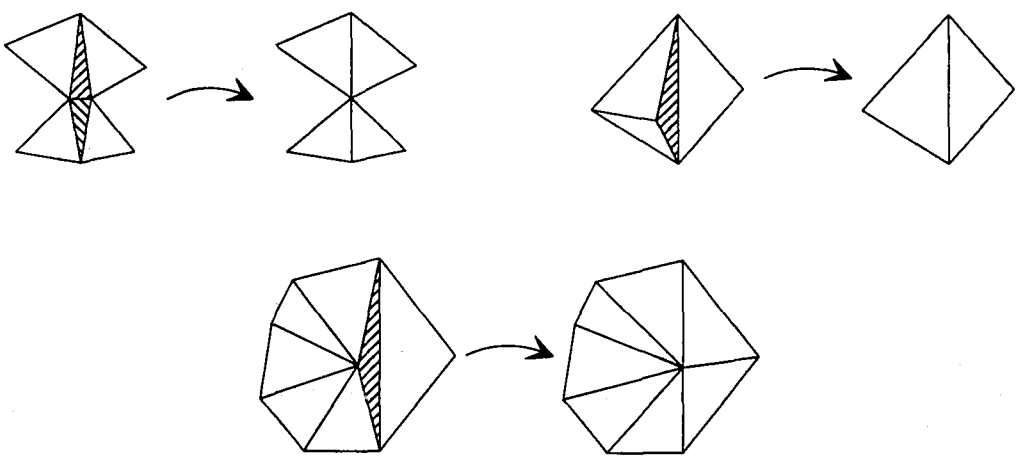

FIGURE 9. Eliminating degeneracies.

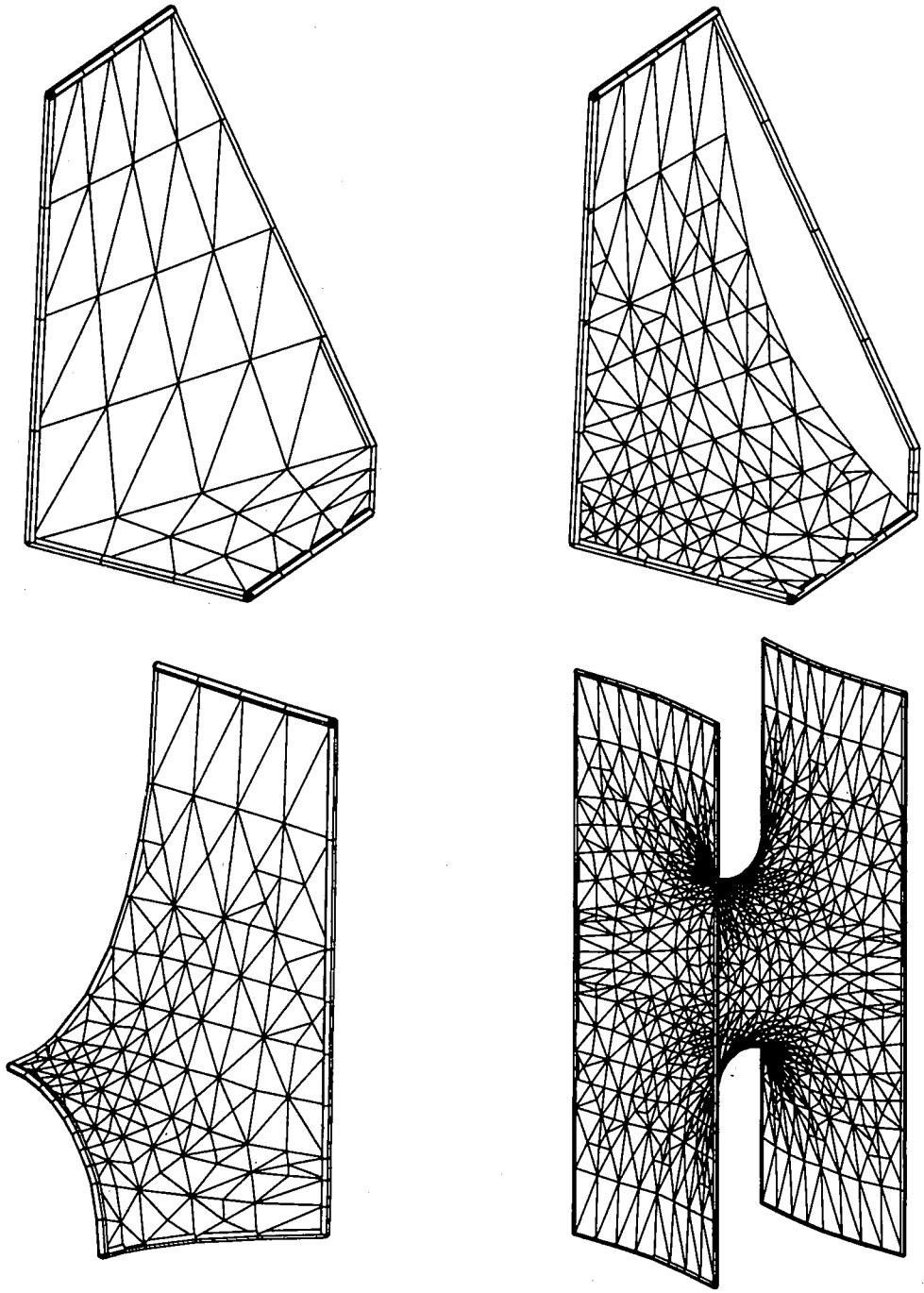

FIGURE 10. Constructing Karcher's Scherk surface with handle [Karcher 1988]. Top left: Initial triangulation with one planar and four straight boundary arcs. Boundary points may vary along the straight arcs and within the planes of the planar arcs. Top right: Triangulation after some minimization steps. Bottom left: The result of the conjugation algorithm has one straight and four planar symmetry arcs. Bottom right: Successive reflection along symmetry lines leads to a fundamental domain for the translation group of the complete minimal surface of Karcher. Refining was controlled by using discrete curvature information of the discrete surface.

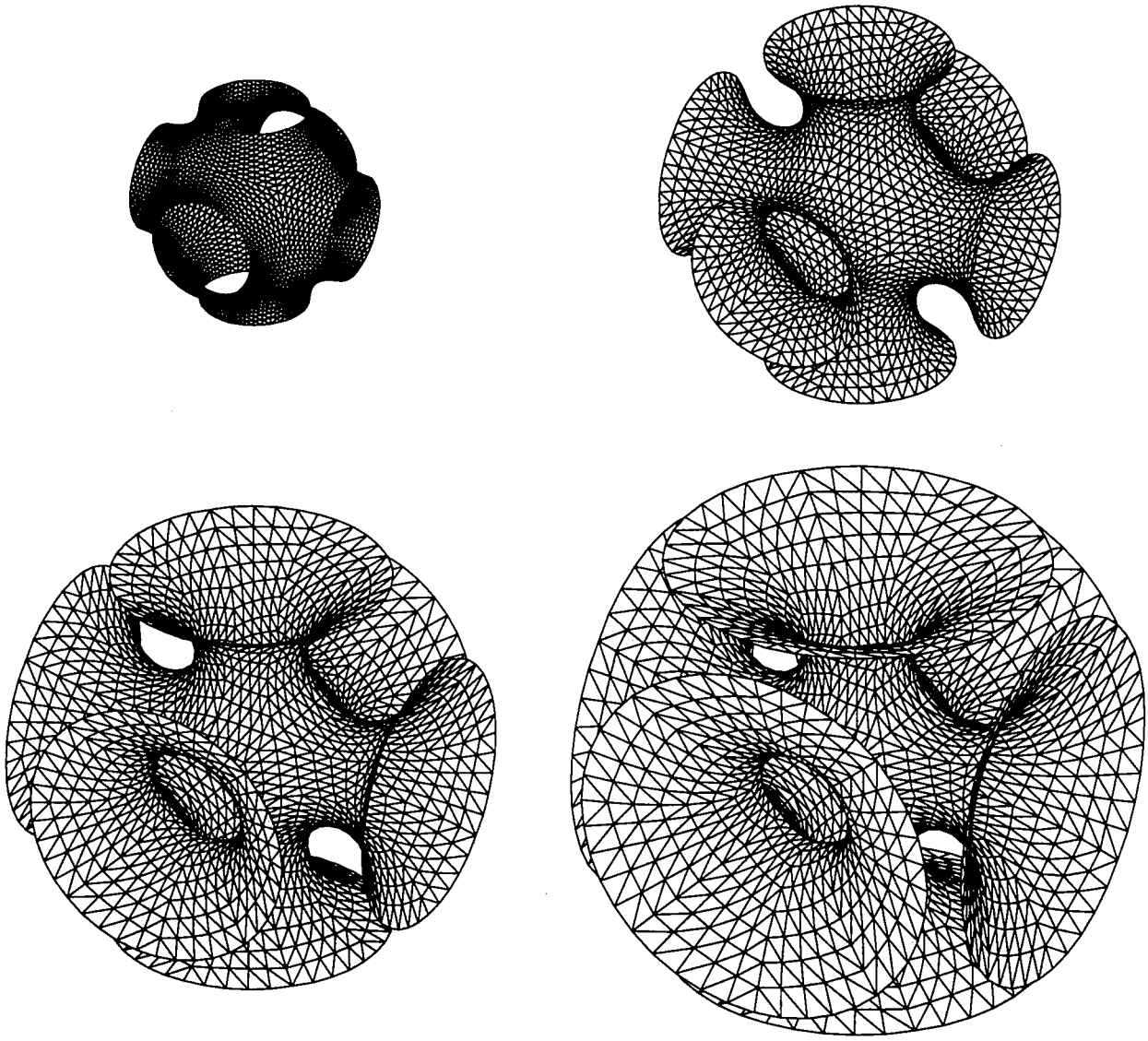

FIGURE 11. Minimal surface with ends. Each of the surfaces in this sequence has cubical symmetry, and is made up of 48 copies of a four-sided fundamental domain, three of whose sides are planar symmetry curves meeting at 60° and 90° angles; the fourth side meets at 90° angles, and is not a symmetry curve. The fundamental domains are obtained by minimizing and conjugating an initial surface (not shown) bounded by three straight lines and a helicoidal arc, also meeting at 60°, 90°, 90° and 90° angles. As the helicoidal arc is translated to infinity, the conjugate grows a flare, or catenoidal end, and becomes an infinite discrete minimal surface in the limit.

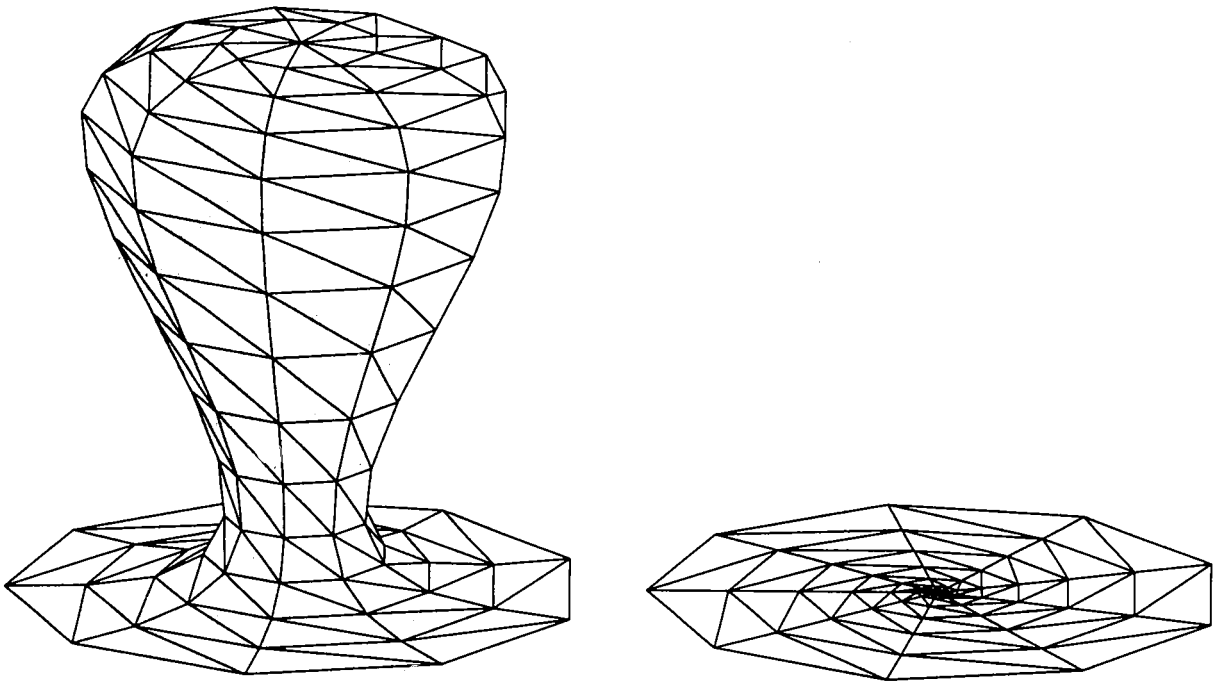

FIGURE 12. Minimizing a drop-like surface, bounded by a planar curve. One minimization step leads directly to a planar surface, and therefore avoids a singularity at the thin neck, expected under mean curvature flow algorithms. This illustrates that the minimization algorithm proceeds discretely also in the time direction.

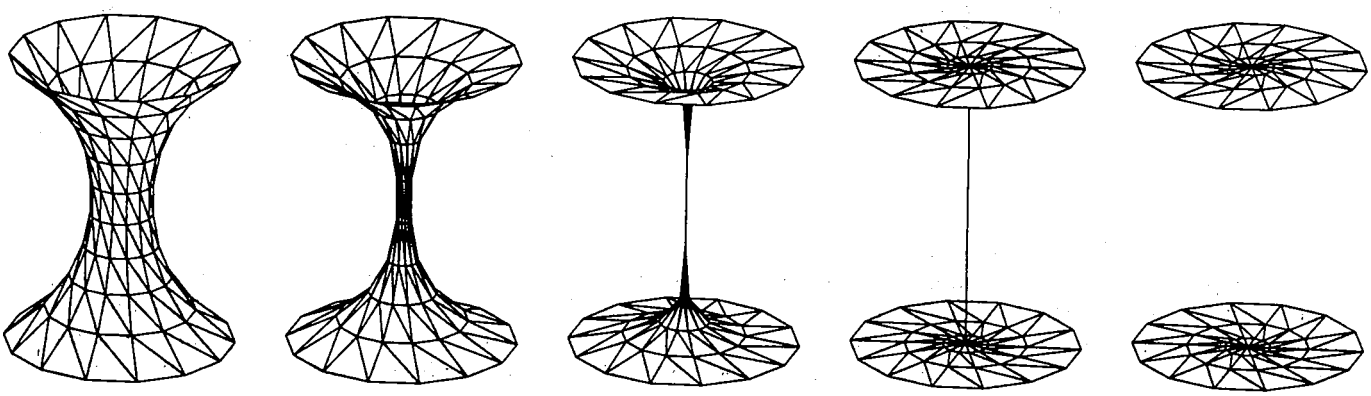

FIGURE 13. The Goldschmidt solution. Three minimization steps are sufficient to transform the initial surface (far left) into the so-called Goldschmidt solution (middle right). Between this and the final figure an additional algorithm was applied to remove degenerate triangles.

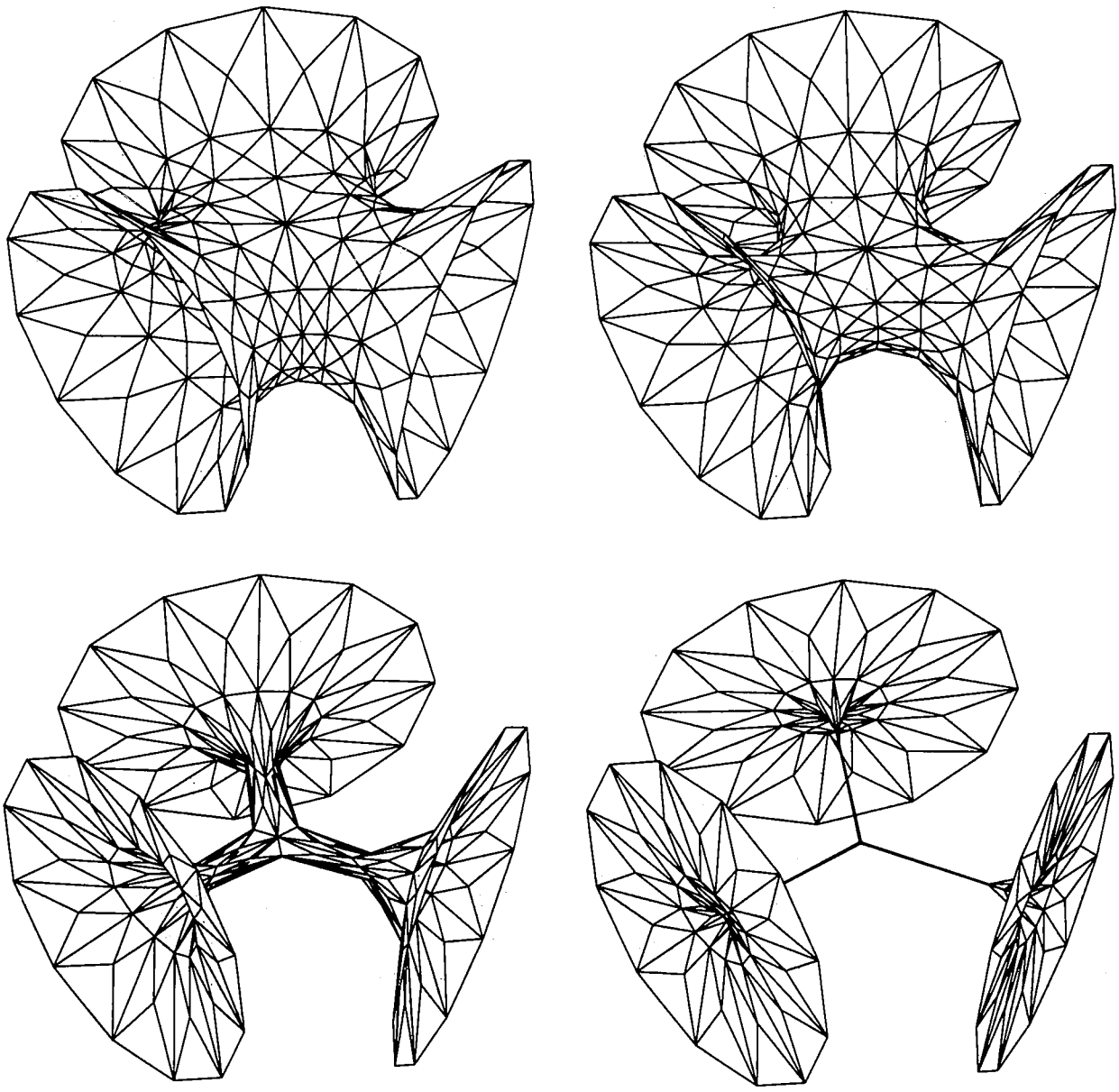

FIGURE 14. Minimizing the instable trinoid. An example similar to Figure 13, but with higher genus. An instable part of the trinoid minimal surface of Jorge and Meeks [1983] was computed using the Weierstraß representation formula and was then used as an initial surface for the minimization algorithm. The same Goldschmidt type solution appears as in Figure 13.

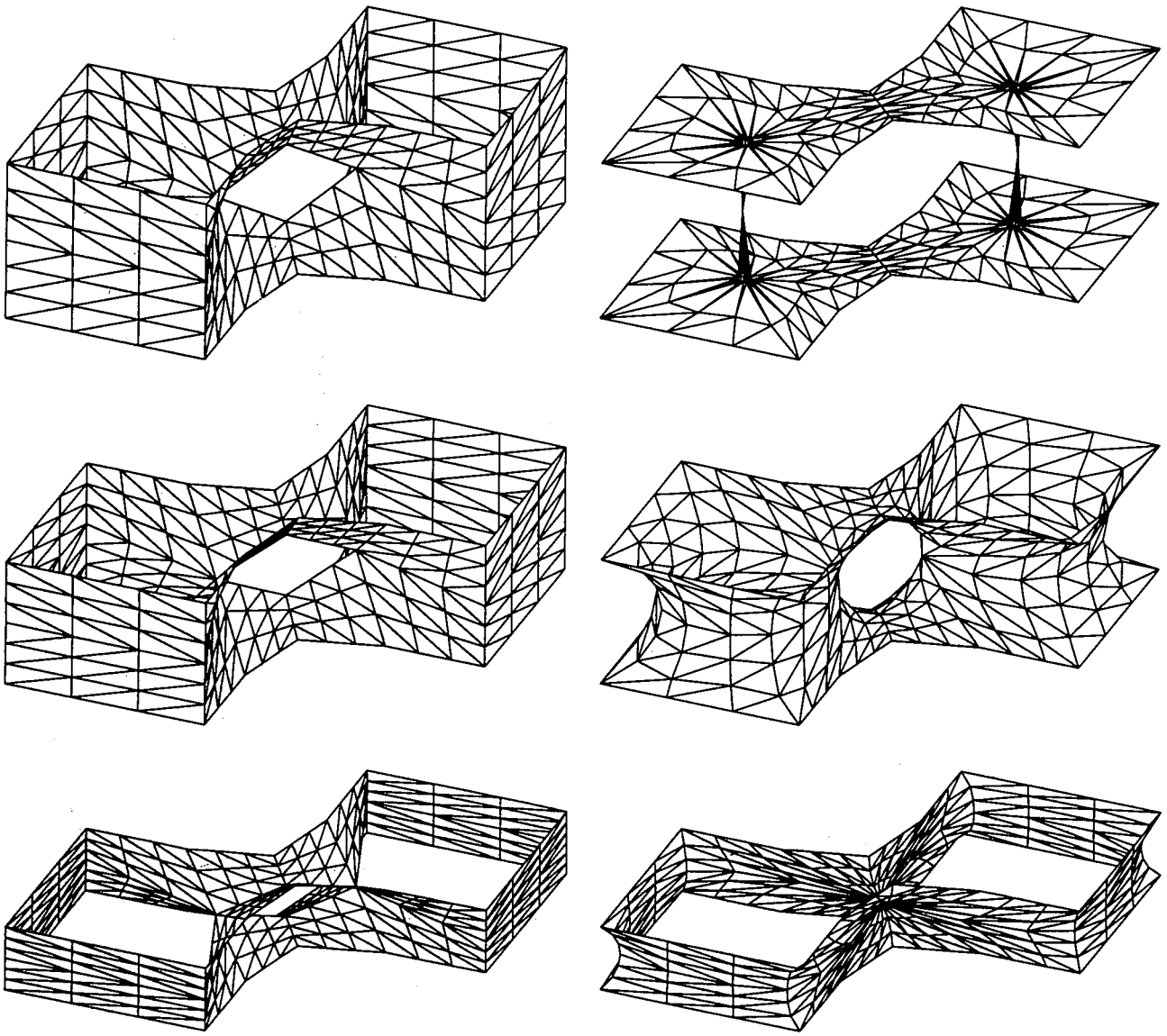

FIGURE 15. Left: A one-parameter family of initial surfaces with the topology of the twice-punctured torus, and varying height (distance between the figure-eight boundary curves). Right: Minimal surfaces after minimization. Depending on the height, three outcomes are possible: two thin necks, with singularities, joining flat pieces (top); one singularity pinching together two opposite points on a cylinder (bottom); or a stable discrete minimal surfaces is obtained in the limit, for special values of the height (middle). The initial surfaces were generated using the surface builder module of Grape.

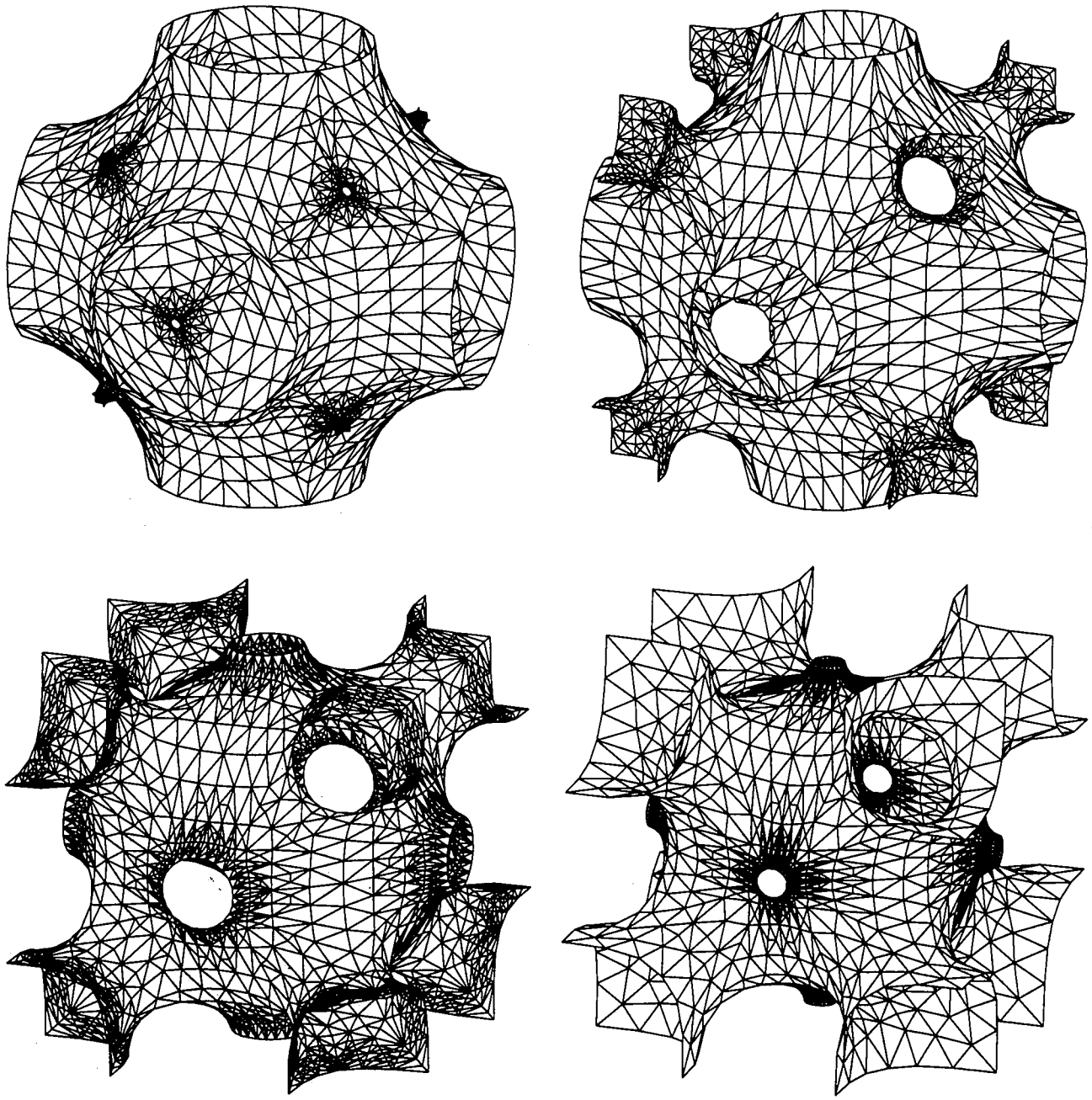

FIGURE 16. Growing Karcher handles. This example illustrates the time-dependent process of growing additional handles out of existing minimal surfaces. For the O,C-TO surface of A. Schoen no representation formula is known; its existence was proved by Karcher [1989] by means of an intermediate-value argument using the conjugate surface construction: roughly, during the process of growing handles there is one value for which the handles meet the existing symmetry planes of the cube. The occurring extreme situations made it necessary to refine adaptively during the deformation. Refining was controlled by using discrete curvature information about the surface.

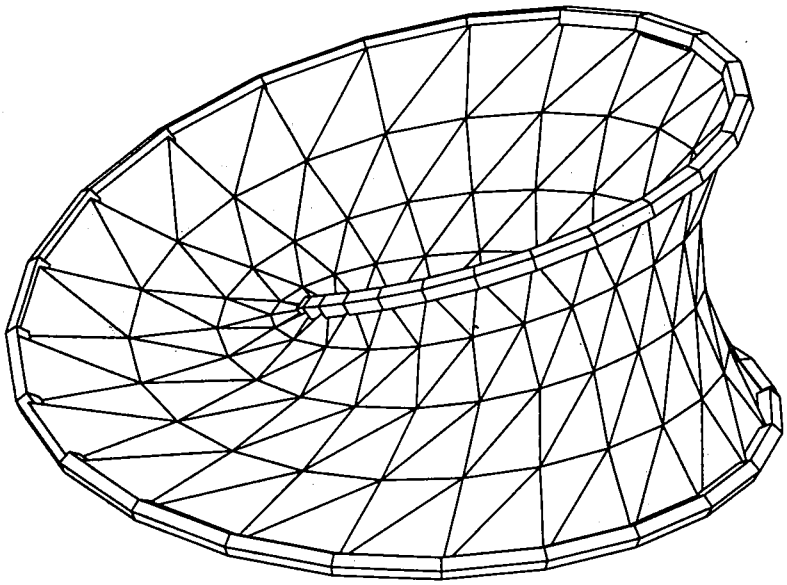

FIGURE 17. A minimal Möbius band. The algorithm handles nonorientable surfaces since the Dirichlet minimality condition (3.2) is independent of the orientation.

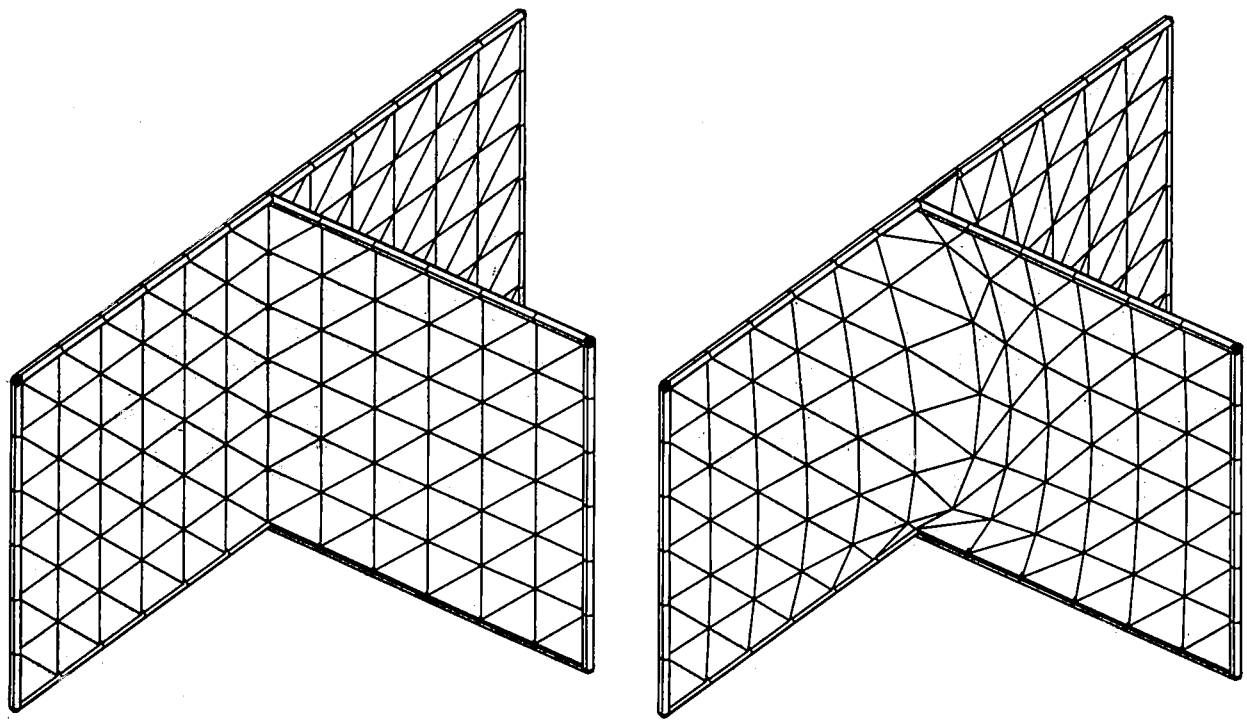

FIGURE 18. A minimal configuration with a singular triple line. Such multiple lines are naturally covered by the algorithm, since the Dirichlet minimality condition at a point (3.2) is a finite sum of the weighted directions of all edges emanating from a point. The weight of each edge is determined by all triangles—possibly more than two—sharing this edge.

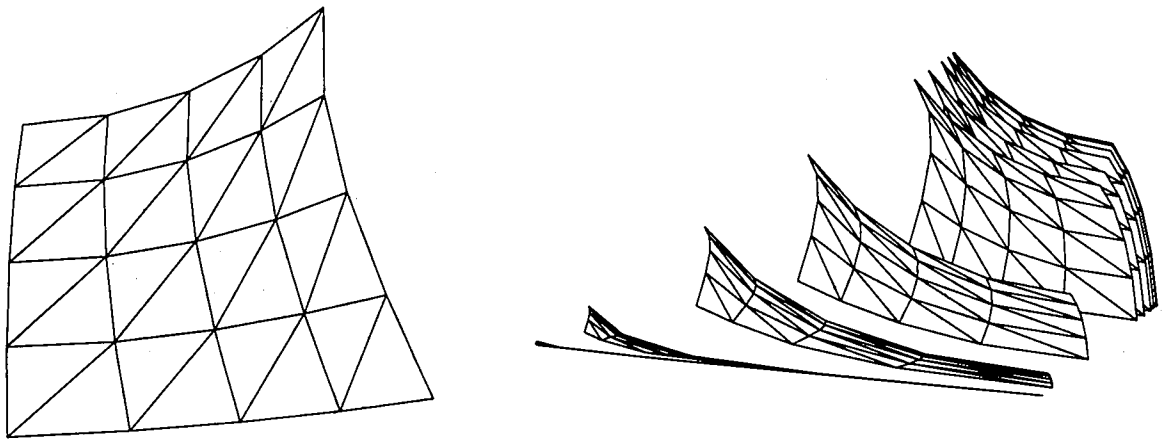

FIGURE 19. Examples showing the first usage of the conjugate surface construction by B. Smyth [1984]. A discrete minimal surface in a quadrilateral is conjugated to a patch bounded by the four faces of a tetrahedron along planar symmetry lines. But this patch is not a stable discrete minimal surface. Further minimization of this patch while keeping the boundary curves restricted to the faces makes the patch degenerate to an edge of the tetrahedron.

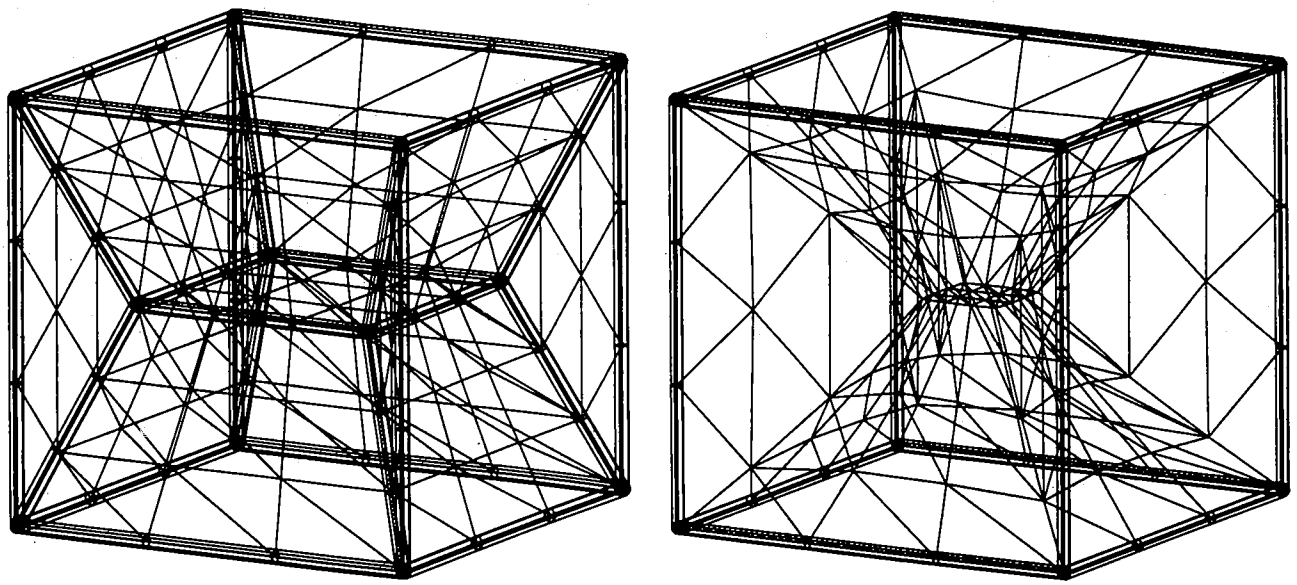

FIGURE 20. A minimal configuration bounded by the edges of a cube. The interior of the surface contains triple lines where surface patches meet at 120° angles.

REFERENCES

[Brakke 1992] K. A. Brakke, "The Surface Evolver", *Experimental Math.* **1** (1992), 141–165.

[Concus 1967] P. Concus, "Numerical solution of the minimal surface equation", *Math. Comput.* **21** (1967), 340–350.

[Courant 1950] R. Courant, *Dirichlet's Principle, Conformal Mapping, and Minimal Surfaces*, Interscience, New York, 1950.

[Douglas 1931] J. Douglas, "Solution of the problem of Plateau", *Trans. Amer. Math. Soc.* **33** (1931), 263–321.

[Dziuk 1991] G. Dziuk, "An algorithm for evolutionary surfaces", *Numer. Math.* **58** (1991), 603–611.

[Hutchinson 1991] J. E. Hutchinson, "Computing Conformal Maps and Minimal Surfaces", *Proc. Centr. Math. Anal.* (Canberra) **26** (1991), 140–161.

[Jorge and Meeks 1983] L. P. M. Jorge and W. H. Meeks, "The topology of complete minimal surfaces of finite total curvature", *Topology* **22** (1983), 203–221.

[Karcher 1988] H. Karcher, "Embedded minimal surfaces derived from Scherk's examples", *Manuscr. Math.* **62** (1988), 83–114.

[Karcher 1989] H. Karcher, "Triply periodic minimal surfaces of Alan Schoen and their constant mean curvature companions", *Manuscr. Math.* **64** (1989), 291–357.

[Karcher et al. 1988] H. Karcher, U. Pinkall and I. Sterling, "New minimal surfaces in S^3", *J. Diff. Geom.* **28** (1988), 169–185.

[Lawson 1970] H. B. Lawson, "Complete minimal surfaces in S^3", *Ann. of Math.* **92** (1970), 335–374.

[Plateau 1873] J. A. F. Plateau, *Statique Expérimentale et Théorétique des Liquides Soumis aux Seules Forces Moléculaires*, Gauthiers-Villars, Paris, 1873.

[Polthier 1991] K. Polthier, "New periodic minimal surfaces in H^3", *Proc. Centr. Math. Anal.* (Canberra) **26** (1991), 201–210.

[Radó 1930] T. Radó, "The problem of least area and the problem of Plateau", *Math. Zeit.* **32** (1930), 763–796.

[Smyth 1984] B. Smyth, "Stationary minimal surfaces with boundary on a simplex", *Invent. Math.* **76** (1984), 411–420.

[Sullivan 1990] J. M. Sullivan, "A crystalline approximation theorem for hypersurfaces", Ph.D. dissertation, Princeton University, 1990.

[Wilson 1961] W. L. Wilson, "On discrete Dirichlet and Plateau problems", *Num. Math.* **3** (1961), 359–373.

[Wohlrab 1985] O. Wohlrab, "Zur numerischen Behandlung von parametrischen Minimalflächen mit halbfreien Rändern", Dissertation, Universität Bonn, 1985.

Ulrich Pinkall, Technische Universität Berlin, Sonderforschungsbereich 288, Straße des 17. Juni, 1000 Berlin 12, Germany (ulrich@sfb288.math.tu-berlin.de)

Konrad Polthier, Mathematisches Institut Universität Bonn, Sonderforschungsbereich 256, Beringstraße 4, 5300 Bonn 1, Germany (polthier@uni-bonn.de)

Received March 2, 1993; accepted April 28